Journal of Metals, Materials and Minerals, 36(3), e2549, 2026

Sustainable lightweight foams from hazardous aluminum dross

Chayapat WEERAPAKDEE[1], Makoto NANKO[2,*], Yen-Ling KUO[2], Sukasem WATCHARAMAISAKUL[1], Kaito SUZUKI[2], Seiryu SUZUKI[2], and Siriwan CHOKKHA[1,*]

[1] *Suranaree University of Technology , School of Ceramic Engineering, Institute of Engineering, Nakhon Ratchasima, 30000, Thailand*
[2] *Nagaoka University of Technology, High Temperature Materials Laboratory, Mechanical Engineering, Nagaoka, Niigata, 940-2188, Japan*

***Corresponding author e-mail**: nanko@mech.nagaokaut.ac.jp, siriwan@sut.ac.th

Received date:
30 October 2025
Revised date:
8 December 2025
Accepted date:
16 February 2026

Keywords:
Aluminum dross;
Ceramic foam;
Sustainable materials;
Industrial waste upcycling

Abstract

Aluminum dross is a hazardous byproduct from aluminum industry that causes environmental problems and high disposal cost. This work presents a sustainable route to upcycle secondary aluminum dross into lightweight ceramic foams for insulating refractory applications. Secondary aluminum dross powder was blended with polyethylene (PE) pore-forming agents (30 vol% to 70 vol%) and polyvinyl alcohol (PVA) binder added as a 7.5 wt% aqueous solution (binder contents: 1 vol% and 3 vol%), followed by pressing and sintering at 1400°C. Increasing PE systematically reduced bulk density and increased open porosity. At 70 vol% PE, the foams reached a bulk density of 0.94 g·cm^{-3} and open porosity of ~74%, satisfying the Japanese Industrial Standard (JIS) specification for lightweight refractory bricks. The maximum compressive strength was ~2 MPa, sufficient for thermal insulation where load-bearing capacity is secondary. X-ray diffraction confirmed a multiphase matrix of α−Al_2O_3, $MgAl_2O_4$, and $CaAl_{12}O_{19}$, indicating solid-state reactions between alumina and Mg/Ca-bearing phases. Morphology revealed a well-connected porous network stabilized by reaction-bonded bridges, indicating strong interparticle bonding and limited pore coalescence during sintering. This approach can divert over 1000 kg of hazardous waste per ton of secondary aluminum dross processed and cut CO_2 emissions by 65% versus alumina routes. The approach promotes circular economy through waste-derived ceramics.

1. Introduction

Aluminum dross is the ash-like skim that forms on the surface of molten aluminum during melting, holding, refining, and recycling. It contains oxides, salts, and entrained metal droplets, and is commonly categorized as “white” (primary) or “black” (secondary) dross depending on the processing route [1]. With the rapid growth of aluminum production, dross generation has increased significantly. The global production of aluminum dross is estimated at approximately 5 million tons each year, corresponding to 7.6% of total aluminum output [2,3]. Without proper treatment, this waste can cause severe environmental problems. For example, AlN and Al_4C_3 can react with moisture to release hazardous gases such as NH_3 and CH_4. In addition, soluble salts in the dross can leach into soil and groundwater, creating long-term contamination risks. Although industries often pay substantial fees for hazardous waste disposal, frequently several hundred USD per ton, the most common management strategy remains landfilling by licensed contractors [3,4].

In practice, landfilling transfers the problem rather than solving it, since buried dross continues to emit toxic gases and leachates over time. Such practices create hidden environmental liabilities and underscore the urgent need for sustainable and permanent valorization strategies. In many countries, regulations now restrict simple landfilling of dross, further motivating industries to seek alternative management solutions [4,5]. Thus, the safe and sustainable utilization of aluminum dross has become both an environmental necessity and an industrial challenge.

The ceramic-forming oxide content in secondary aluminum dross (SAD) offers a promising opportunity for sustainable valorization. Because SAD is rich in Al_2O_3 and contains Mg- and Ca-bearing species, it can serve as a feedstock for engineered ceramics when reactive phases are appropriately managed [6]. Globally, SAD is generated at approximately 1 million tons per year and typically contains high concentrations of Al_2O_3, MgO, and CaO [2]. Disposal costs can reach ~200 USD per ton. However, untreated dross not only incurs high management costs but can also continue to release hazardous gases and leach soluble salts into surrounding environments. Beyond conventional metal recovery, prior studies have explored dross in refractories and other structural materials, leveraging Al_2O_3–MgO–CaO chemistries to form α-Al_2O_3/$MgAl_2O_4$ frameworks bonded by calcium aluminates [7]. These considerations highlight the need for conversion strategies that transform dross into functional ceramic materials while reducing environmental impact.

Several studies have investigated the reuse of SAD in ceramic and construction applications. For example, Chokkha *et al.* engineered porous geopolymers by exploiting aluminum-waste–driven foaming, where the Al–water reaction generated an interconnected macropore network. The authors reported a monotonic rise in porosity with increasing waste addition together with compressive strengths in the

~1 Mpa to 6 MPa range (SEM confirmed open cells and XRD showed the typical geopolymer gel matrix), highlighting a low-temperature route to lightweight structural panels [2]. Li *et al.* evaluated dross as a reactive alumina source for high-alumina refractories: after pretreatments to remove deleterious species, dross-derived powders were co-fired to form α-Al_2O_3/$MgAl_2O_4$-bonded matrices; densification improved, apparent porosity decreased, and room-temperature strength increased relative to mixes without the dross-derived reactants, demonstrating that SAD can function as an active ceramic former rather than only as inert filler [8]. Lin *et al.* converted aluminum dross to calcined Al_2O_3 using microwave-plasma processing; the rapid, high-enthalpy environment shortened residence times, reduced energy input compared with conventional calcination, and produced high-purity alumina while lowering nitride/fluoride residues—thereby supplying a cleaner ceramic feedstock for downstream refractories [9]. Ramaswamy and co-workers showed practical incorporation of dross into refractory bodies made from industrial waste streams; shaped products sintered to acceptable bulk density and cold-crushing strength, and the study emphasized manufacturability (mixing/pressing/sintering windows) and cost reduction without sacrificing baseline thermo-mechanical performance [3]. These findings demonstrate the versatility of SAD in engineering applications. However, most prior work has focused on dense, non-porous products, leaving a critical gap in the development of lightweight foam ceramics specifically optimized for thermal insulation and energy-efficient applications.

Lightweight foam ceramics represent a compelling solution to this gap. These materials are characterized by reduced bulk density (0.3 $g \cdot cm^{-3}$ to 1.0 $g \cdot cm^{-3}$) and interconnected pore networks, which significantly lower thermal conductivity (0.05 $W \cdot m^{-1} \cdot K^{-1}$ to 0.2 $W \cdot m^{-1} \cdot K^{-1}$) while retaining high-temperature stability [10,11]. Porous ceramics are particularly attractive for thermal insulation application, as reducing bulk density and tailoring open porosity can lower thermal conductivity while maintaining thermal and mechanical stability [10]. Among available processing strategies, sacrificial pore former provides simple, scalable, and effective routes. Polyethylene (PE) powders are widely used as sacrificial pore formers due to their clean burnout and controllable particle size distribution [12]. In parallel, polyvinyl alcohol (PVA) binders enhance green strength and facilitate granulation, enabling robust shaping prior to burnout and sintering. By combining PE pore formers with PVA binders, SAD can be transformed into thermally stable, lightweight cellular ceramics with tunable porosity and compressive strength. While previous studies demonstrate the potential of dross reuse, systematic approaches for optimizing processing parameters to achieve lightweight foams with controlled pore architecture and mechanical stability remain lacking

In this study, lightweight insulating foams are produced from SAD using polyethylene (PE) powders as sacrificial pore formers and polyvinyl alcohol (PVA) as a binder. The green bodies are pressed and sintered to form an interconnected, thermally stable cellular microstructure. Bulk density, open porosity and the compressive strength are measured to establish processing–structure–property relationships. This approach provides a sustainable route to convert hazardous SAD into thermally insulating, lightweight ceramics suitable for industrial applications.

2. Experimental procedure

2.1 Material preparation

SAD was used as the main ceramic feedstock. High-purity α-Al_2O_3 powder was processed under identical conditions and served as the reference material. The α-Al_2O_3 powder was selected to have a particle size comparable to that of the milled SAD powder, to ensure a fair comparison of processing and sintering behavior.

Polyethylene (PE) powders in two commercial grades were used as sacrificial pore-forming agents: PE A (Flowthene®) and PE B (Flowbeads®). The physical properties of the two PE grades are summarized in Table 1. These two grades were compared to investigate how differences in PE particle size and particle morphology influence pore formation and the subsequent sintering response. Supplier datasheets did not specify molecular weight or glass transition temperature (T_g); therefore, the comparison in this study focuses on the listed physical parameters.

A 7.5 wt% PVA aqueous solution was used as the binder. Here, "7.5 wt%" refers to the PVA concentration in the binder solution, whereas the binder addition (1 vol% and 3 vol%) refers to the amount of the PVA solution added to the batch formulation, as summarized in Table 2. Mixtures were prepared with PE contents of 30 vol%, 50 vol%, and 70 vol% and binder additions of 1 vol% and 3 vol%.

The as-received SAD was ball-milled prior to mixing to reduce particle size and improve homogeneity; no sieving/classification step was applied before or after milling. SAD powder and PE pore-formers were first dry-blended to ensure homogeneous mixing. The PVA solution was then gradually added to obtain a cohesive, free-flowing granulate.

Cylindrical specimens were produced by uniaxial pressing in a 15 mm-diameter die at 5 MPa for 30 s. After pressing, specimens were carefully ejected and inspected for lamination and edge defects; specimens with visible cracking or lamination were excluded. Specimen uniformity was controlled by targeting a final (sintered) specimen height within 11 mm to 15 mm (height/diameter ≈ 0.73 to 1.0) to minimize buckling effects during compression testing. No post-sintering height machining was performed to avoid introducing processing-induced cracks. Only minor edge dressing was applied when necessary (e.g., to improve wetting for Archimedes measurements).

Thermal processing was conducted in air using a three-step schedule designed to remove organics, generate porosity, and consolidate the oxide network. Specimens were first dried at 80°C for 18 h, then heated to 300°C and held for 2 h for binder removal and pore initiation, and finally sintered at 1400°C for 3 h followed by furnace cooling. During sintering, pellets were placed on inert setters with sufficient spacing to ensure uniform heating and effective off-gassing.

2.2 Characterization of lightweight foams

Phase identification was performed by X-ray diffraction (XRD) using ground fragments from all samples. XRD of the dried precursor was conducted to determine the initial crystalline phases, repeated after sintering to identify newly formed phases and evaluate phase evolution. Measurements were carried out using a Rigaku MiniFlex 600 diffractometer operated at 40 kV and 15 mA with Cu Kα radiation (λ = 1.5406 Å). Data were collected over a 2θ range of 20° to 80° with a step size of 0.02° and a scan rate of 2.0°·min^{-1}. Particular attention was given to α-Al_2O_3, $MgAl_2O_4$, and calcium-aluminate phases.

Table 1. Physical properties of polyethylene (PE) pore-forming agents used in this study.

PE	A	B
Density (JIS K7112) [g·cm^{-3}]	0.919	0.919
Powder size [μ m]	≦30	6-25
Melting point [℃]	106	105

Table 2. Mix design (vol%) for aluminum-dross (AD) and alumina foams.

Sample	Composition [vol%]				
	AD	Al_2O_3	PE (A)	PE (B)	PVA
	70	0	30	0	1
SAD A 1%	50	0	50	0	1
	30	0	70	0	1
	70	0	30	0	3
SAD A 3%	50	0	50	0	3
	30	0	70	0	3
	70	0	0	30	1
SAD B 1%	50	0	0	50	1
	30	0	0	70	1
	70	0	0	30	3
SAD B 3%	50	0	0	50	3
	30	0	0	70	3
	0	70	30	0	1
Alumina A 1%	0	50	50	0	1
	0	30	70	0	1
	0	70	30	0	3
Alumina A 3%	0	50	50	0	3
	0	30	70	0	3
	0	70	0	30	1
Alumina B 1%	0	50	0	50	1
	0	30	0	70	1
	0	70	0	30	3
Alumina B 3%	0	50	0	50	3
	0	30	0	70	3

Bulk density and open porosity were measured by the Archimedes method. Prior to measurement, pellet edges were lightly dressed to improve wetting. The dry mass (M_{dry}), saturated mass in air (M_{wet}), and immersed mass in water (M_{in}) were recorded. Using the water density (ρ_w) at the measurement temperature, bulk density (ρ) and open porosity (P_o) were calculated as Equation (1) and Equation (2):

$$\rho = \rho_w \times (M_{dry} / (M_{wet} - M_{in})) \quad (1)$$

$$P_o = (M_{wet} - M_{dry}) / (M_{wet} - M_{in}) \quad (2)$$

Compressive strength was measured using a universal testing machine at a crosshead speed of 0.5 mm·min^{-1}, following ASTM C133 (cold-crushing strength of refractories) [13]. Each specimen was loaded until failure, and the maximum load was recorded. The nominal compressive strength was calculated by dividing the maximum load by the loaded area. Fracture surfaces were collected for subsequent microscopic examination.

Scanning electron microscopy (SEM; Hitachi FlexSEM 1000 II) was used to observe fracture surfaces and evaluate pore morphology (pore size, connectivity, and ligament features) across different pore-former grades and contents. Prior to imaging, samples were coated with a thin gold layer to improve conductivity. SEM imaging was conducted at an accelerating voltage of 15 kV at a magnification of 2000x. Representative micrographs were collected from at least three regions of each specimen to ensure reproducibility [14].

Finally, bulk density and open porosity were plotted as functions of pore-former content to establish the processing–structure relationship. Compressive strength was plotted versus open porosity to quantify the structure–property trade-off. The primary target was to achieve bulk densities below 1.0 g·cm^{-3}, suitable for lightweight insulation applications. The overall processing route is schematically illustrated in Figure 1.

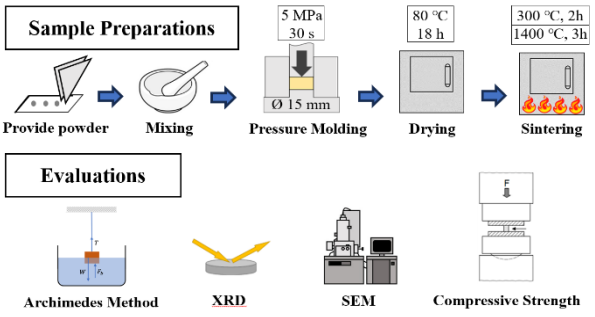

Figure. 1. Schematic of the overall processing route.

3. Results and discussion

3.1 Chemical composition analysis by XRF

The chemical compositions of the starting powders (SAD and α-Al_2O_3) were quantified by XRF and are summarized in Table 3 as oxide compositions (mass%). The SAD feedstock is alumina-rich (Al_2O_3 = 77.2 mass%) but contains substantial MgO (10.6 mass%) and measurable CaO (1.66 mass%), together with minor oxides such as SiO_2, K_2O, MnO, Fe_2O_3, and trace amounts of CuO, ZnO, SrO, and ZrO_2. In contrast, the α-Al_2O_3 reference powder shows a much higher Al_2O_3 content (96.6 mass%) with only minor Na_2O (0.408 mass%), Fe_2O_3 (0.0291 mass%), and trace Ga_2O_3 (0.0105 mass%), while MgO and CaO were not detected (ND).

The presence of MgO and CaO in SAD is important because these oxides can react with alumina during firing at 1400°C to form refractory secondary phases (e.g., $MgAl_2O_4$ spinel and $CaAl_{12}O_{19}$ calcium hexaluminate). Thus, the XRF results provide direct chemical evidence supporting the multiphase development observed in the XRD patterns and help explain differences in sintering behavior and structural evolution between SAD-derived foams and phase-pure alumina foams. Minor impurity oxides in SAD may also influence local liquid formation and neck growth during sintering, which could affect pore-wall consolidation and macroscopic integrity at high PE contents.

3.2 Macroscopic integrity and appearance

SAD specimens preserved coherent cylindrical shapes across 30 vol% to 70 vol% PE (Table 2). Even at 70 vol% PE, the SAD foams could be handled without crumbling, indicating sufficient integrity in both the green and sintered states. In contrast, alumina specimens became fragile at the highest PE content, and several compacts fragmented during handling. This difference is consistent with the reduced framework stability of single-phase cellular ceramics at very high porosity [11]. These macroscopic observations suggest that the multiphase SAD-derived framework may provide improved shape retention during processing and handling. Maintaining specimen integrity at 70 vol% PE is also advantageous for scale-up because it can reduce losses during post-processing and transportation, which is beneficial for lightweight thermal-insulation components.

For clarity, in Table 1-2, PE A corresponds to Flowthene® and PE B corresponds to Flowbeads®. Based on the macroscopic photographs, no systematic difference in overall shape integrity was observed between PE A and PE B under the same PE content and binder condition. Instead, macroscopic stability was governed primarily by PE volume fraction and the base raw material (SAD vs alumina). Any PE-grade-related effects are expected to be more apparent at the microstructural level (e.g., pore morphology and ligament formation) rather than in macroscopic handling behavior, and are therefore discussed in the subsequent sections.

3.3 Density–porosity evolution with PE addition

To quantify the effect of pore-former content on foam structure, bulk density (ρ) and open porosity (P_o) were plotted as functions of PE content (vol%). The density results are shown in Figure 2(a) for 1 vol% PVA and Figure 2(b) for 3 vol% PVA, while the corresponding porosity results are shown in Figure 3(a) and Figure 3(b), respectively. Two PE grades were used: PE A (Flowthene®) and PE B (Flowbeads®) (Table 1). Accordingly, samples prepared using PE A are denoted SAD-A and Alumina-A, whereas those using PE B are denoted SAD-B and Alumina-B (Table 2).

Across all systems, increasing PE content from 30 vol% to 70 vol% led to a monotonic decrease in bulk density and a monotonic increase in open porosity. For SAD-based foams, bulk density decreased approximately linearly with PE addition (Figure 2(a,b)), giving representative values of 1.34 g·cm^{-3}, 1.19 g·cm^{-3}, and 0.94 g·cm^{-3} at 30 vol%, 50 vol%, and 70 vol% PE, respectively. The corresponding open porosity values increased from 62% to 67% and 74% (Figure 3 (a,b)). Importantly, the 70 vol% PE condition achieved $\rho < 1.0$ g·cm^{-3}, meeting the lightweight-insulation target for insulating refractory applications. These trends are consistent with cellular-solids relationships linking relative density and porosity [11] and with prior reports on porous ceramics derived from SAD [7].

Table 3. Chemical compositions of SAD and α-Al_2O_3 starting powders measured by XRF (reported as oxides, mass%; ND = not detected or below the reporting limit).

Oxide	SAD [mass%]	α-Al_2O_3 [mass%]
CO_2	8.26	2.92
Na_2O	ND	0.408
MgO	10.6	ND
Al_2O_3	77.2	96.6
SiO_2	1.09	ND
SO_3	0.232	ND
Cl	0.0291	ND
K_2O	0.289	ND
CaO	1.66	ND
MnO	0.164	ND
Fe_2O_3	0.280	0.0291
CuO	0.0514	ND
ZnO	0.0628	ND
SrO	0.0070	ND
ZrO_2	0.0090	ND
Ga_2O_3	ND	0.0105

Table 4. Macroscopic photographs of sintered specimens at 30 vol%, 50 vol%, and 70 vol% PE.

Sample	Polyethylene content [vol%]		
	30	50	70
SAD A 1%	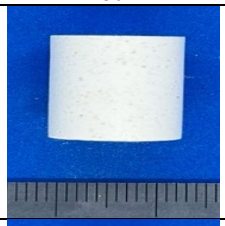	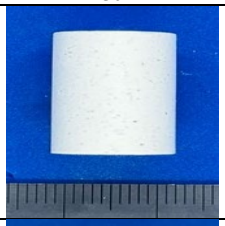	
SAD A 3%	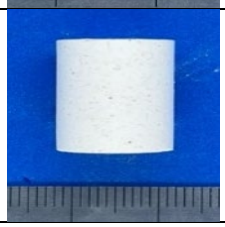	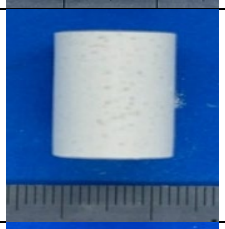	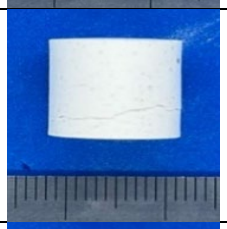
SAD B 1%	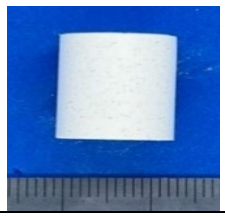		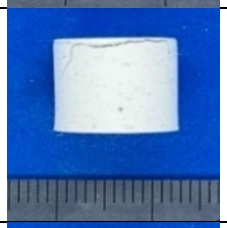
SAD B 3%	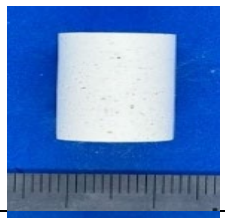	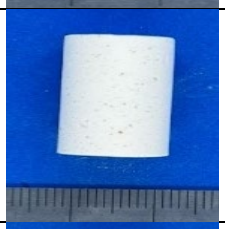	
Alumina A 1%	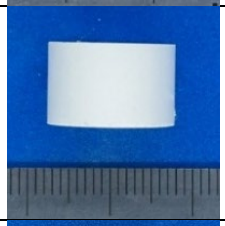	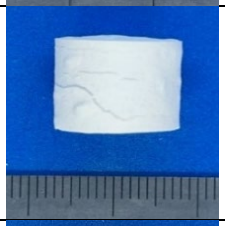	
Alumina A 3%	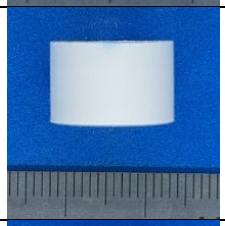	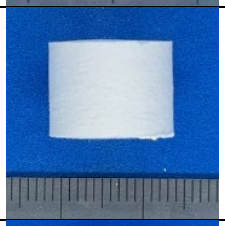	
Alumina B 1%	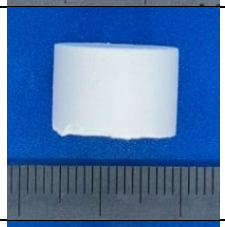	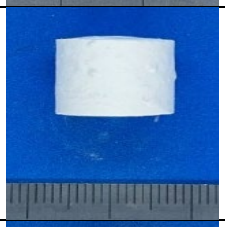	
Alumina B 3%	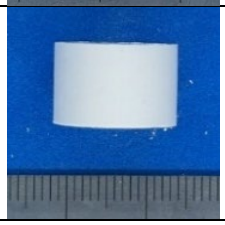	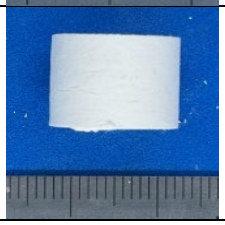	

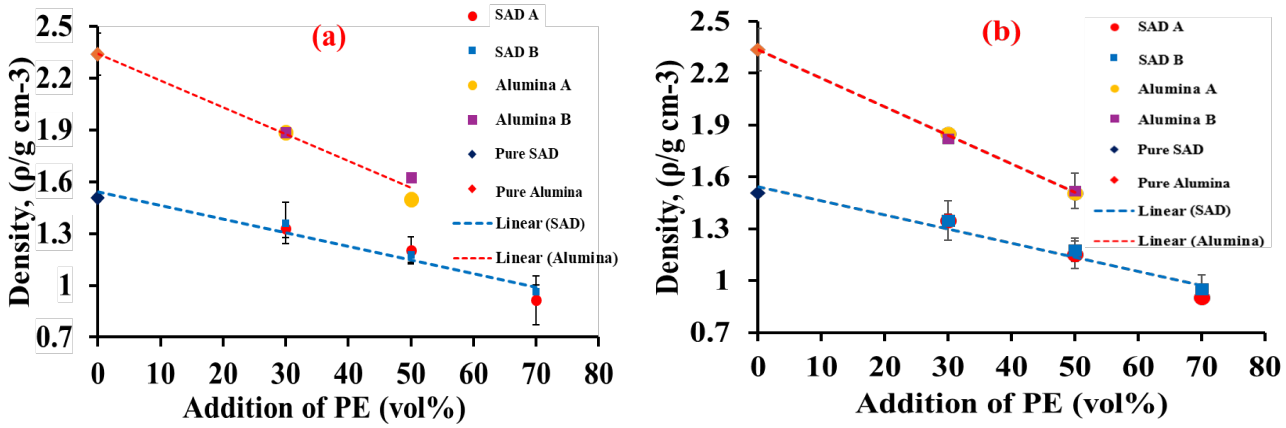

Figure 2. Effect of PE addition (vol%) on bulk density (ρ, g·cm⁻³) of SAD and Alumina foams prepared with different PVA contents: (a) 1 vol% PVA and (b) 3 vol% PVA.

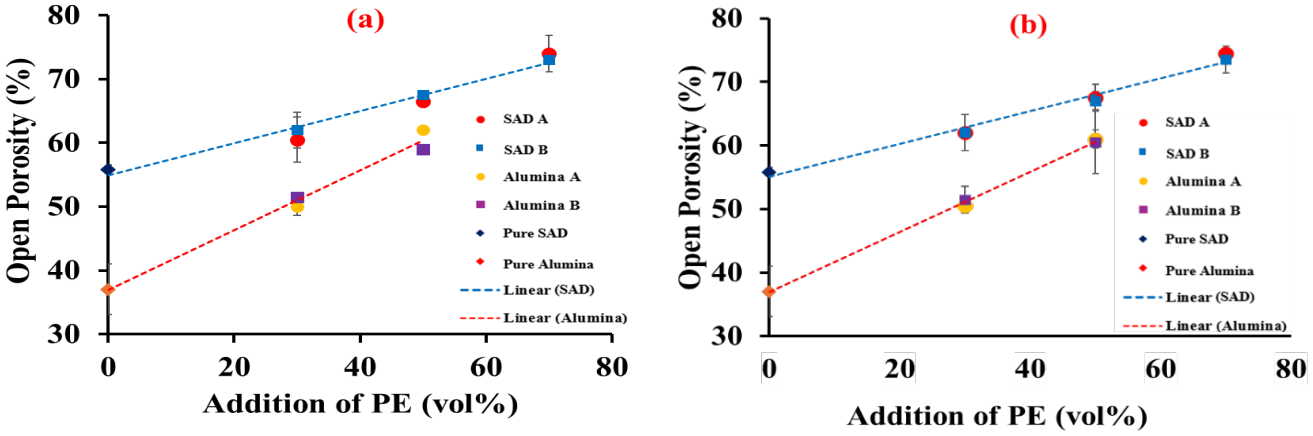

Figure 3. Effect of PE addition (vol%) on open porosity (P_o, %) of SAD and Alumina foams prepared with different PVA contents: (a) 1 vol% PVA, and (b) 3 vol% PVA.

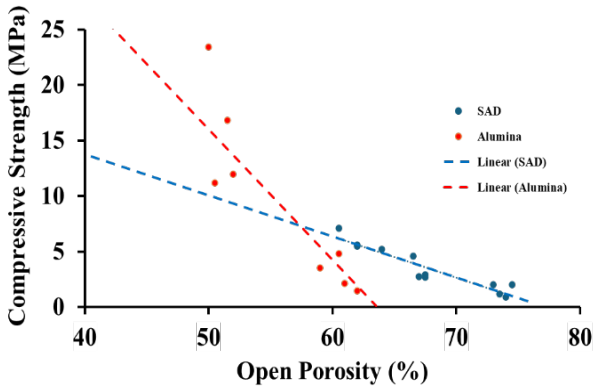

Figure 4. Compressive strength vs open porosity: comparison between SAD and Alumina.

3.4 Strength–porosity trade-off

Compressive strength decreased with increasing open porosity in both systems (Figure 4). For SAD-based foams, the data are mainly distributed from ~60% to ~74% porosity, where strength decreases gradually from approximately ~6 MPa to 7 MPa near ~60% to 62% to ~2 MPa to 4 MPa near ~65% to 68% and ~1 MPa to 2 MPa near ~73% to 74%. In contrast, alumina foams show much higher strength at lower porosity (approximately ~11 MPa to 23 MPa at ~50% to 52% porosity) but a markedly steeper reduction with increasing porosity, approaching near-zero strength by ~62% to 63% porosity. This behavior is consistent with brittle cellular solids [11]. Compressive strength was measured following ASTM C133 [13].

Figure 4 is intentionally presented as a strength–porosity plot to highlight the intrinsic relationship between compressive strength and open porosity, regardless of the pore-former type. Therefore, PE grade (A/B) and PE content are not emphasized in Figure 4, because the objective is to compare strength at a given porosity rather than to distinguish pore-former sources. The influence of PE addition is shown separately in Figure 5(a) (1 vol% PVA) and Figure 5(b) (3 vol% PVA).

As shown in Figure 5(a), the compressive strength of SAD-A decreased from 6.37 MPa at 30 vol% PE to 3.75 MPa at 50 vol% PE and 1.45 MPa at 70 vol% PE, while SAD-B followed a similar decreasing trend. In Figure 5(b), SAD-A showed strengths of approximately 5.49 MPa (30 vol% PE), 2.66 MPa (50 vol% PE), and 2.04 MPa (70 vol% PE), again with a comparable trend for SAD-B. Alumina foams exhibited higher strengths at 30 vol% PE (typically ~11 MPa to 17 MPa depending on grade), but their strength dropped sharply at 50 vol% PE (on the order of ~2 MPa to 5 MPa), and specimens at 70 vol% PE were too fragile for reliable testing, consistent with the rapid decline observed in Figure 4.

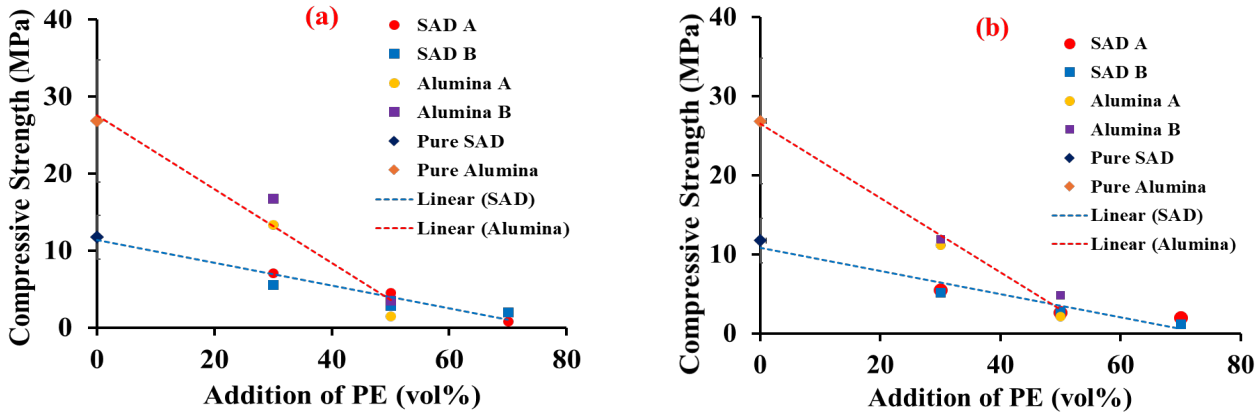

Figure 5. Effect of PE addition (vol%) on compressive strength (MPa) of SAD and Alumina foams prepared with different PVA contents: (a) 1 vol% PVA and (b) 3 vol% PVA.

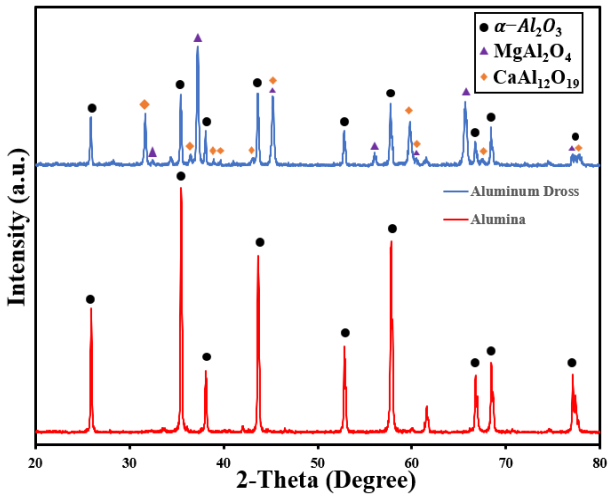

Figure 6. XRD patterns for SAD and Alumina. SAD exhibits a multiphase matrix composed of α-Al_2O_3, $MgAl_2O_4$ and $CaAl_{12}O_{19}$. Alumina shows a single-phase α- Al_2O_3 matrix.

In contrast, alumina foams exhibited a steeper density decrease and porosity increase with PE addition (see Figure 2(a,b) and Figure 3 (a,b)). Representative values indicate that increasing PE content from 30 to 50 vol% reduced bulk density from 1.85 to 1.55 g·cm^{-3} while increasing open porosity from 50.5% to 60%. This behavior suggests faster void opening and/or coalescence in the single-phase alumina framework for a given pore-former increment, consistent with typical behavior of brittle cellular ceramics at high porosity [11]. (Values at 70 vol% PE are not included for alumina because several compacts fragmented during handling at the highest PE content.).

When comparing PE grades, SAD-A vs SAD-B and Alumina-A vs Alumina-B follow the same overall trends in both the density–PE relationships (Figure 2(a,b)) and the porosity–PE relationships (Figure 3(a,b)). Within the present scatter, no systematic separation between PE A and PE B is evident in these bulk properties at a fixed PE content and PVA level. This indicates that PE volume fraction is the dominant factor governing bulk density and open porosity, whereas the influence of PE grade is secondary for these macroscopic metrics. Any PE-grade-related effects are therefore expected to be more apparent in pore morphology (e.g., pore size/shape distribution and ligament formation) rather than in averaged bulk density/porosity values, and are discussed in the microstructural section.

Notably, SAD-based foams show a smaller sensitivity of open porosity to PE content (i.e., a gentler porosity–PE slope in Figure 3 (a,b)) than alumina foams. This means that the same change in PE content produces a smaller change in open porosity and thus enables finer control of the final pore structure. This reduced sensitivity may be associated with the multiphase nature of SAD, where reaction-derived bonding and rigid secondary phases can help restrain void growth during burnout and sintering. This interpretation is consistent with reported phase development in Al_2O_3–MgO–CaO systems derived from aluminum dross [1,4,7,8,15,16].

Finally, the linear trend lines shown in Figure 2(a,b) and Figure 3 (a,b) are least-squares fits included to quantify the sensitivity (slope) of bulk density and open porosity to PE addition for each system and PVA level. The fitted equations are used only to support comparisons within the measured range (30 vol% to 70 vol% PE) and are not intended for extrapolation beyond the experimental domain.

3.5 X-ray Diffraction (XRD)

X-ray diffraction (XRD) patterns of the sintered SAD–derived bodies (Figure 6) show a multiphase ceramic assemblage dominated by α-Al_2O_3 with reaction-formed $MgAl_2O_4$ (spinel) and $CaAl_{12}O_{19}$ (calcium hexaluminate). These phases were identified by matching diffraction peaks to standard reference data: α-Al_2O_3 (JCPDS No. 46-1212, rhombohedral, space group R-3c), $MgAl_2O_4$ (JCPDS No. 21-1152, cubic spinel, space group Fd-3m), and $CaAl_{12}O_{19}$ (JCPDS No. 70-0134, hexagonal, space group $P6_3/mmc$).

The coexistence of these crystalline phases confirms solid-state reactions between alumina and Mg/Ca-bearing species inherently present in secondary aluminum dross during high-temperature sintering at 1400°C [1,4,7,8]. The formation of $MgAl_2O_4$ and $CaAl_{12}O_{19}$ indicates that MgO and CaO, originating from flux residues and alloying additives in erfthe dross, diffused into the alumina lattice, promoting intacial reactions according to Equation (3) and Equation (4):

$$MgO + Al_2O_3 \rightarrow MgAl_2O_4 \quad (3)$$

$$CaO + 6Al_2O_3 \rightarrow CaAl_{12}O_{19} \quad (4)$$

These reactions are thermodynamically favored above 1300°C to 1400°C, as confirmed by previous phase equilibrium studies in the Al_2O_3–MgO–CaO system [15,16]. The spinel ($MgAl_2O_4$) and Calcium Hexaluminate ($CaAl_{12}O_{19}$) phases exhibit high thermal stability and low thermal expansion, which may improve the dimensional stability and thermal-shock resistance of the porous ceramic framework. Their presence within the α-Al_2O_3 matrix can contribute to a more rigid, interlocking microstructure, potentially reducing sintering shrinkage while maintaining mechanical integrity at elevated temperatures [14–16].

In comparison, the reference alumina specimens exhibit only α-Al_2O_3 reflections (JCPDS No. 46-1212), confirming its single-phase structure under identical firing conditions [6,17]. This contrast highlights the compositional reactivity of aluminum dross and its inherent potential as a self-reactive precursor capable of forming functional refractory phases without external additives.

Collectively, these results demonstrate that SAD can be upcycled into a structurally stable and thermally resilient material via in-situ phase formation. This approach supports the broader circular-economy framework by converting a hazardous metallurgical waste into a value-added ceramic with refractory-grade performance.

3.6 Scanning Electron Microscope (SEM)

Scanning electron microscopy (SEM) observations (Table 5) reveal that the SAD foams developed an open-cell porous network, with clear changes in pore morphology as the polyethylene (PE) content increased. At 30 vol% PE, the structure remained relatively dense with small, semi-connected pores. Increasing the PE content to 50 vol% led to more interconnected pores and thinner ligaments, while at 70 vol% PE, the pore walls became rougher and less uniform but the overall framework was still retained-highlighting the structural integrity of SAD even at high porosity. The irregular pore walls and tortuous fracture features indicate multiphase sintering and localized grain bridge. XRD confirmed the presence of $MgAl_2O_4$ and $CaAl_{12}O_{19}$ after sintering; however, their spatial distribution was not examined by elemental mapping in this study. These reaction-formed phases may contribute to the integrity of the multiphase framework and could help suppress excessive pore collapse during polymer burnout and sintering, although this interpretation remains qualitative [7,11,12,15]. Accordingly, these phases are considered to potentially provide a "microstructural anchoring" effect that may improve shape retention and dimensional stability under thermal stress. In addition, samples with highest PVA content (3 vol%) showed smoother and more continuous necks than those with 1 vol% PVA, suggesting that sufficient binder promotes better particle cohesion and reduces cracking during burnout. Taken together, the multiphase grain-bridging structure in SAD foams may improve mechanical reliability compared to single-phase alumina, despite similar porosities. This observation supports the feasibility of transforming aluminum dross, typically considered hazardous waste, into lightweight refractory ceramics aligned with circular-economy and sustainable-materials strategies.

Table 5. SEM microstructures (2000×) of SAD foams at 30, 50, and 70 vol% PE (A/B; PVA 1% and 3%).

Sample	Magnification 2000x		
	Polyethylene content [vol%]		
	30	50	70
SAD A 1%	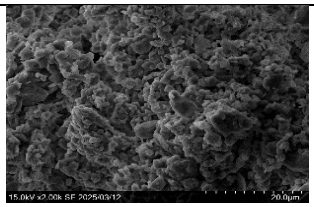	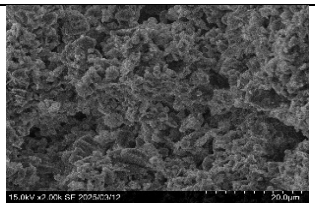	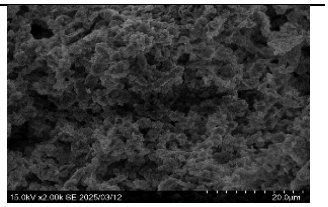
SAD A 3%	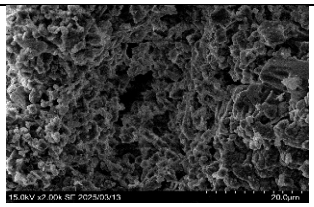	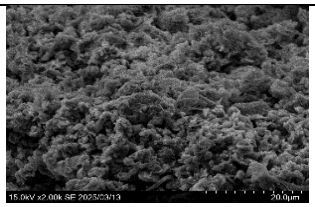	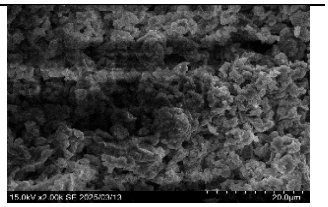
SAD B 1%	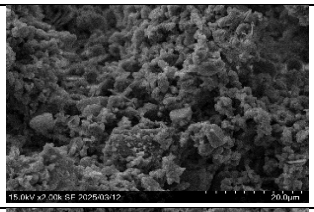	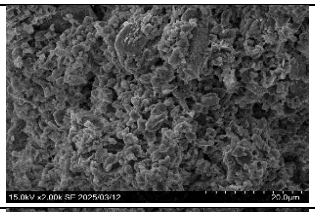	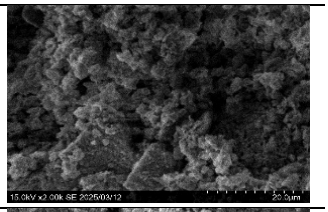
SAD B 3%	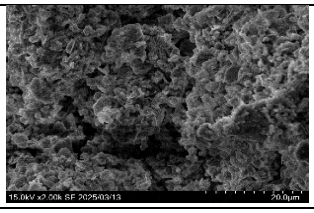	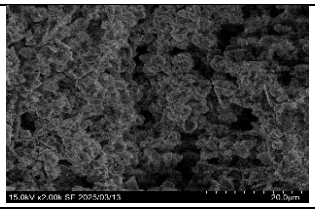	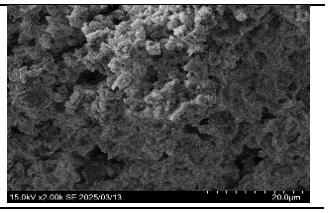

Table 6. SEM microstructures (2000×) of alumina foams at 30 and 50 vol% PE (A/B; PVA 1% and 3%).

Sample	Magnification 2000x	
	Polyethylene content [vol%]	
	30	50
Alumina A 1%	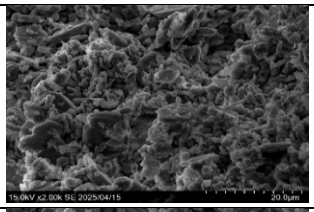	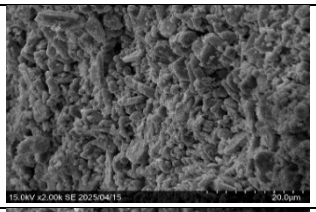
Alumina A 3%	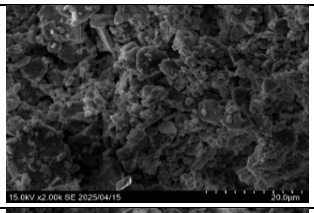	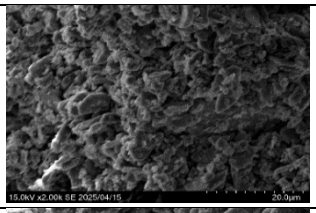
Alumina B 1%	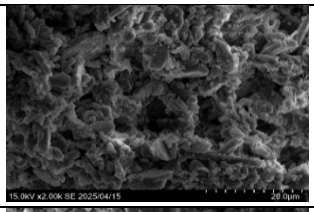	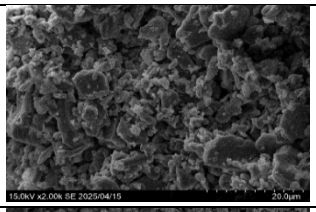
Alumina B 3%	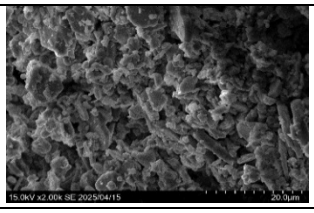	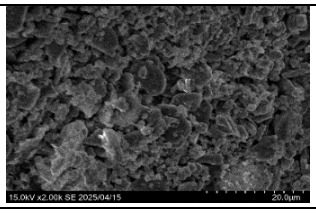

In contrast, the alumina foams exhibited smoother and more homogeneous ligaments than those derived from aluminum dross (Table 6). At 30 vol% PE, the Al_2O_3 foams showed well-connected grains with moderate pore walls; however, as the porosity increased to 50 vol% PE, the ligaments became thinner and locally fractured, resulting in partial wall collapse. The surfaces appeared featureless, indicating limited intergranular diffusion and the absence of secondary phase reinforcement [6,11,12]. Such single-phase morphology is characteristic of pure alumina ceramics, where the lack of thermally stable secondary phases leads to weak neck formation and poor stress transfer across the pore framework. Consequently, higher porosity accelerated microcrack propagation and reduced the structural stiffness of the foams. These microstructural features correspond well with the experimental density–porosity and strength–porosity trends, confirming that the multiphase SAD system retained better macroscopic integrity at high porosity levels [7].

Notably, the SEM appearance of Alumina A (1 vol% PVA, 50 vol% PE) differs from the other alumina conditions. This difference may be related to the lower binder addition (1 vol% PVA), which can reduce granule cohesion during forming and promote local heterogeneity, such as PE-rich regions or non-uniform packing. During burn-out, such heterogeneity may generate localized stresses (e.g., differential shrinkage and gas release), leading to early ligament rupture, micro-cracking, or localized collapse, which would appear as a more disrupted fracture morphology. In addition, fracture-surface SEM is sensitive to the crack path; if the crack preferentially propagates through a weak, PE-rich, or poorly bonded region, the observed microstructure can appear different from the average structure. To minimize sampling bias, multiple fields of view and higher-magnification images should be considered for this specimen.

4. Conclusions

Lightweight ceramic foams were successfully fabricated from SAD using polyethylene (PE) as a sacrificial pore former (30 vol% to 70 vol%) and polyvinyl alcohol (PVA) as a binder (PVA used as a 7.5 wt% aqueous solution; binder addition = 1 vol% and 3 vol%). After pressing and sintering at 1400°C, increasing PE content systematically decreased bulk density and increased open porosity. SAD foams prepared with 70 vol% PE achieved bulk densities below 1.0 $g{\cdot}cm^{-3}$ (0.94 $g{\cdot}cm^{-3}$) and an open porosity of 74%, meeting the target density range for JIS lightweight/insulating refractory bricks. Within the present scatter, no systematic separation in the density–porosity response was observed between PE A (Flowthene®) and PE B (Flowbeads®), indicating that PE volume fraction is the dominant parameter controlling macroscopic pore development. Compressive strength decreased with increasing porosity, consistent with the classical density–strength trade-off in cellular ceramics. For PE-containing SAD foams, strength decreased with increasing PE content, and high-porosity SAD foams (74% porosity) retained compressive strengths on the order of ~1 MPa to 2 MPa (up to ~2 MPa to 3 MPa depending on binder condition), supporting insulating applications where load-bearing capacity is

secondary. Alumina specimens were used as a phase-pure reference. Although alumina can exhibit higher strength at lower porosity, it became fragile at very high porosity under the present processing window. XRD confirmed that SAD-derived bodies form a stable multiphase assemblage of α-Al_2O_3–$MgAl_2O_4$–$CaAl_{12}O_{19}$ after sintering, consistent with solid-state reactions in Al_2O_3–MgO–CaO systems. SEM observations indicate an open-cell porous framework and ligament evolution with increasing PE content. Further work using higher-magnification imaging, polished cross-sections, elemental mapping, and/or 3D pore characterization would be valuable for quantifying pore morphology and phase spatial distribution, and for correlating these descriptors with thermal conductivity and long-term performance for practical JIS-compliant insulating refractories.

Acknowledgements

We thank the Nanko-Kuo Laboratory (Nagaoka University of Technology: NUT) for laboratory access and guidance, the NUT Analysis Center for XRD/SEM support, Sumitomo Seika Chemicals Co., Ltd. for providing Flowthene® and Flowbeads® polyethylene powders, and Suranaree University of Technology's cooperative-education program for administrative assistance; high-temperature processing and microscopy were performed at NUT shared facilities.

References

[1] O. Manfredi, W. Wuth, and I. Bohlinger, "Characterizing the physical and chemical properties of aluminum dross," *JOM*, vol. 49, pp. 48–51, 1997.

[2] S. Chokkha, J. Ayawanna, A. Poowancum, T. Singlaem, and P. Mitsomwang, "Fabrication of porous geopolymers utilizing aluminum wastes as foaming agent," *Journal of Metals, Materials and Minerals*, vol. 34, no. 2, p. 1966, 2014.

[3] P. Ramaswamy, S. A. Gomes, and N. P. Ravichander, "Utilization of aluminum dross: Refractories from industrial waste," *IOP Conference Series: Materials Science and Engineering*, vol. 577, p. 012101, 2019.

[4] A. Meshram, and K. K. Singh, "Recovery of valuable products from hazardous aluminum dross: A review," *Resources, Conservation & Recycling*, vol. 130, pp. 95–108, 2018.

[5] Z. Li, H. Li, X. Huang, W. Wu, Z. Sun, X. Wu, and S. Li, "Removal of nitrides and fluorides from secondary aluminum dross by catalytic hydrolysis and its mechanism," *Heliyon*, vol. 9, no. 1, e12893, 2023.

[6] K. Okada, T. Isobe, K.-i Katsumata, Y. Kameshima, A. Nakajima, and K. J. D. MacKenzie, "Porous ceramics mimicking nature—preparation and properties of microstructures with unidirectionally oriented pores," *Science and Technology of Advanced Materials*, vol. 12, no. 6, Art. 064701, 2011.

[7] W. Li, X. Zhang, J. Zhang, H. Shen, J. Yang, Y. Liu, J. Liu, S. Zhang, and J. Yang, "Porous ceramics with near-zero shrinkage and low thermal conductivity from hazardous secondary aluminum dross," *Journal of the American Ceramic Society*, vol. 105, no. 5, pp. 3197–3210, 2022.

[8] A. Li, H. Zhang, and H. Yang, "Evaluation of aluminum dross as raw material for high-alumina refractory," *Ceramics International*, vol. 40, no. 8, pp. 12585–12590, 2014.

[9] W.-C. Lin, C.-H. Tsai, D.-N. Zhang, S.-S. Syu, and Y.-M. Kuo, "Recycling of aluminum dross for producing calcinated alumina by microwave plasma," *Sustainable Environment Research*, vol. 32, no. 1, Art. 50, 2022.

[10] J. Liu, S. Zhang, H. Shen, B. Lou, and B. Zhang, "Recycling of secondary aluminum dross to make alumina by hydrometallurgy: A review," *Journal of Materials Research and Technology*, vol. 32, pp. 4234–4245, 2024.

[11] L. J. Gibson, and M. F. Ashby, "Cellular solids: Structure and properties, 2nd ed. Cambridge, UK: Cambridge University Press, 1997.

[12] R. M. Khattab, M. M. S. Wahsh, and N. M. Khalil, "Preparation and characterization of porous alumina ceramics through starch consolidation casting technique," *Ceramics International*, vol. 38, no. 6, pp. 4723-4728, 2012.

[13] *Standard Test Methods for Cold Crushing Strength and Modulus of Rupture of Refractories*, ASTM C133-97(2021), ASTM International, West Conshohocken, PA, 2021.

[14] M. N. Rahaman, "Engineering & Technology, Physical Sciences," in *Ceramic Processing and Sintering*, 2nd ed. New York, NY: Marcel Dekker, 2003, page 875.

[15] F. Wang, J. Ye, G. He, G. Liu, Z. Xie, and J. Li, "Preparation and characterization of porous $MgAl_2O_4$ spinel ceramic supports from bauxite and magnesite," *Ceramics International*, vol. 41, no. 6, pp. 7374–7380, 2015.

[16] J.-H Chen, H.-Y. Chen, M. Yan, Z. Cao, and W.-J. Mi, "Formation mechanism of calcium hexaluminate," *International Journal of Minerals, Metallurgy and Materials*, vol. 23, no. 10, pp. 1225–1230, 2016.

[17] B. D. Cullity, and S. R. Stock, *Elements of X-Ray Diffraction, 3rd ed*. Upper Saddle River, NJ: Prentice Hall, 2001, page 696.